MAPK phosphatase-1 facilitates the loss of oxidative myofibers associated with obesity in mice

Rachel J. Roth,[1] Annie M. Le,[1] Lei Zhang,[1] Mario Kahn,[2] Varman T. Samuel,[2,3] Gerald I. Shulman,[2,4] and Anton M. Bennett[1]

[1]Department of Pharmacology, [2]Department of Cellular and Molecular Physiology, [3]Department of Internal Medicine, Section of Endocrinology and Metabolism, and [4]Howard Hughes Medical Institute, Yale University School of Medicine, New Haven, Connecticut, USA.

Oxidative myofibers, also known as slow-twitch myofibers, help maintain the metabolic health of mammals, and it has been proposed that decreased numbers correlate with increased risk of obesity. The transcriptional coactivator PPARγ coactivator 1α (PGC-1α) plays a central role in maintaining levels of oxidative myofibers in skeletal muscle. Indeed, loss of PGC-1α expression has been linked to a reduction in the proportion of oxidative myofibers in the skeletal muscle of obese mice. MAPK phosphatase-1 (MKP-1) is encoded by *mkp-1*, a stress-responsive immediate-early gene that dephosphorylates MAPKs in the nucleus. Previously we showed that mice deficient in MKP-1 have enhanced energy expenditure and are resistant to diet-induced obesity. Here we show in mice that excess dietary fat induced MKP-1 overexpression in skeletal muscle, and that this resulted in reduced p38 MAPK–mediated phosphorylation of PGC-1α on sites that promoted its stability. Consistent with this, MKP-1–deficient mice expressed higher levels of PGC-1α in skeletal muscle than did wild-type mice and were refractory to the loss of oxidative myofibers when fed a high-fat diet. Collectively, these data demonstrate an essential role for MKP-1 as a regulator of the myofiber composition of skeletal muscle and suggest a potential role for MKP-1 in metabolic syndrome.

Introduction

The MAPK pathway plays a critical role in physiological and pathophysiological processes. The growth factor–responsive Erks (Erk1 and Erk2) and the stress-responsive MAPKs (p38 MAPK and JNK) are established regulators of signaling pathways that control diverse cellular processes (1–3). The MAPKs are pleiotropic in action and function to phosphorylate multiple protein targets, in both a spatial and a temporal manner (4). The activities of the MAPKs are regulated by their upstream activators, the MAPK kinases (MKK), which phosphorylate and activate the MAPKs on regulatory threonine and tyrosine residues (1–3, 5). The major mechanism through which MAPKs are inactivated occurs by the actions of the MAPK phosphatases (MKPs), which dephosphorylate the MAPKs on their regulatory residues (6, 7). Hence, aberrant regulation of MAPK activity can arise through defective activation by upstream signaling pathways and/or by defective regulation of the MKPs (8). Much has been learned about the participation of upstream pathways that activate the MAPKs and their role in disease (9). Although the role of the MKPs in disease has been emerging (10–12), there is still much to be learned about how the MKPs play a role in pathophysiological signaling.

Largely through genetic efforts, it has been established that the MKPs play essential physiological roles in the negative regulation of the MAPKs (7, 12, 13). Using mice deficient for MKP-1, a nuclear localized immediate-early MKP, we previously showed that the activities of the MAPKs were upregulated in insulin-responsive tissues, demonstrating that MKP-1 plays an essential physiological role in the negative regulation of the MAPKs (14). In those studies, we demonstrated that MKP-1 plays an important role in the regulation of energy expenditure, and that mice lacking MKP-1 expression are resistant to diet-induced obesity. Surprisingly, even though these *mkp-1*$^{-/-}$ mice are resistant to diet-induced obesity, they still succumb to impairment of insulin action when fed a high-fat diet (HFD; ref. 14). We attributed this to the observation that MKP-1 dephosphorylates the pool of activated MAPKs in the nucleus, rather than the cytoplasmic pool of MAPKs, which target the proximal components of the insulin pathway (14). Hence, MKP-1 plays an essential role in the regulation of the nuclear pool of MAPKs important for metabolic homeostasis. The mechanism for how MKP-1 exerts its effect on metabolic signaling still remains to be defined, and whether MKP-1 is involved in the progression of metabolic disease remains unknown.

Skeletal muscle is the major source of energy expenditure in the rodent (15–17), and defects in skeletal muscle oxidative metabolism have been implicated in numerous metabolic pathologies, including insulin resistance, glucose intolerance, and obesity (15, 17). Oxidative capacity of skeletal muscle is determined by mitochondrial content and controlled by nervous system inputs, calcium flux, and transcriptional events (15). Although the majority of skeletal muscle fibers are glycolytic (also referred to as fast-twitch), those that are oxidative (also referred to as slow-twitch) are important for overall metabolic wellness (16). Therefore, depending upon physiological demand, the oxidative capacity of skeletal muscle can decrease during periods of inactivity or HFD feeding or increase in response to exercise. It has been proposed that decreases in oxidative skeletal muscle fiber type content correlates with an increased risk of obesity (15). Indeed, obese individuals have been found to exhibit decreases in oxidative and increases in glycolytic myofibers (18, 19). However, the pathway through which HFD feeding induces loss of oxidative myofiber composition remains unclear.

Conflict of interest: The authors have declared that no conflict of interest exists.
Citation for this article: *J. Clin. Invest.* **119**:3817–3829 (2009). doi:10.1172/JCI39054.

Numerous proteins have been identified that control skeletal muscle fiber type establishment, maintenance, and oxidative capacity. Among the most notable of these is the transcriptional coactivator PPARγ coactivator 1α (PGC-1α), which has previously been shown to regulate mitochondrial biogenesis and oxidative metabolism in skeletal muscle (20, 21). The importance of PGC-1α in skeletal muscle function has been revealed through studies using PGC-1α transgenic mouse models (22). PGC-1α overexpression in skeletal muscle of these transgenic mice exhibit increased levels of oxidative myofibers (22). In contrast, mice lacking PGC-1α in skeletal muscle demonstrate a shift from oxidative to glycolytic myofibers (23). Consistent with the supposition that oxidative myofibers play important roles in metabolic homeostasis, it has previously been shown that PGC-1α expression levels are inversely correlated with plasma free fatty acids (FAs) and risk of developing metabolic syndrome (24–26). It has been proposed that PGC-1α downregulation, induced either by HFD feeding in mice or by exposure of FAs to muscle cells, occurs through a MEK- or p38 MAPK–dependent pathway (27, 28). PGC-1α expression and activity are increased as a result of p38 MAPK–mediated phosphorylation of PGC-1α, which serves to stabilize the protein (29, 30). However, whether the changes in MAPK activity during obesity are involved in the downregulation of PGC-1α and subsequently the loss of oxidative myofiber composition has yet to be fully established.

In the present study, we provide evidence that MKP-1 plays a critical role in mediating the switch from oxidative to glycolytic myofibers during HFD feeding. We suggest that MKP-1 mediates this response through negatively regulating PGC-1α expression, by inactivating p38 MAPK–mediated phosphorylation of PGC-1α on sites that promote its stability. We determined that MKP-1 was a transcriptional target for FAs and was induced upon HFD feeding, which suggests that when overexpressed, MKP-1 might trigger PGC-1α downregulation. These results provide evidence that MKP-1 plays a central role in the regulation of myofiber composition and possibly obesity.

Results

Resistance to diet-induced obesity and increased energy expenditure in mkp-1$^{-/-}$ mice. Previously, we showed that mice originally derived on a 129/J × C57BL6/J background that lack expression of MKP-1 (*mkp-1$^{-/-}$* mice; ref. 31) were resistant to diet-induced obesity (14). To determine the susceptibility of genetic variation for this phenotype, we backcrossed *mkp-1$^{-/-}$* mice on a 129/J × C57BL6/J background on to a pure C57BL6/J background for 8 generations, and the body weights of the C57BL6/J *mkp-1$^{-/-}$* mice were analyzed over 6 months. In contrast to our previous results for 129/J × C57BL6/J *mkp-1$^{-/-}$* mice (14), the C57BL6/J *mkp-1$^{-/-}$* mice displayed equivalent changes in weight gain on a chow diet over a 6-month period compared with *mkp-1$^{+/+}$* mice (Supplemental Figure 1; supplemental material available online with this article; doi:10.1172/JCI39054DS1). However, we found that C57BL6/J *mkp-1$^{-/-}$* mice were resistant to weight gain when fed the HFD (Figure 1A). We subjected these mice to spectroscopic analysis to measure whole body fat and lean mass. C57BL6/J *mkp-1$^{-/-}$* mice had a total body weight that was 18% less than C57BL6/J *mkp-1$^{+/+}$* mice after 16 weeks on a HFD ($P < 0.01$; Figure 1B). Although we observed a slight decrease in lean muscle mass in C57BL6/J *mkp-1$^{-/-}$* mice (9%; $P < 0.05$), a striking reduction in total body adiposity was observed in C57BL6/J *mkp-1$^{-/-}$* mice compared with C57BL6/J *mkp-1$^{+/+}$* mice after 16 weeks on a HFD (43%; $P < 0.05$; Figure 1B). We found that, similar to 129/J × C57BL6/J *mkp-1$^{-/-}$* mice, C57BL6/J *mkp-1$^{-/-}$* mice exhibited significantly increased levels of both oxygen consumption (17%; $P < 0.05$) and energy expenditure (17%; $P < 0.05$) compared with C57BL6/J *mkp-1$^{+/+}$* mice after 16 weeks on a HFD (Figure 1, C and D). Moreover, despite being resistant to diet-induced obesity, C57BL6/J *mkp-1$^{-/-}$* mice were hyperphagic (Figure 1E) and showed levels of locomotor activity equivalent to those of C57BL6/J *mkp-1$^{+/+}$* mice (Figure 1F). Hence, the effects of MKP-1 deficiency on total body mass were independent of food intake and locomotor activity, but dependent upon the control of energy expenditure. That both mixed and pure-bred mice lacking MKP-1 exhibited similar phenotypes strongly suggests that the resistance to diet-induced obesity is an intrinsic property of MKP-1 rather than influenced by genetic background. C57BL6/J *mkp-1$^{+/+}$* and C57BL6/J *mkp-1$^{-/-}$* mice were used throughout this study, and are referred to herein as *mkp-1$^{+/+}$* and *mkp-1$^{-/-}$* mice, respectively.

FAs stimulate MKP-1 transcriptional activity in skeletal muscle. To examine the basis for the resistance to diet-induced obesity, and hence gain insight into a potential role for MKP-1 in obesity, we assessed whether expression of MKP-1 is altered when mice are fed a HFD. Our previous study suggested that MKP-1 could affect energy expenditure in skeletal muscle, based upon the observation that mice lacking MKP-1 exhibited enhanced levels of skeletal muscle mitochondrial oxygen consumption (14). Given that skeletal muscle is a primary source of energy expenditure (15–17), we hypothesized that MKP-1 expression levels in skeletal muscle change during HFD feeding. We found that *mkp-1* mRNA levels from skeletal muscle increased by 50% within the first 2 weeks of initiating the HFD (Figure 2A). These levels increased over time and became significantly elevated compared with those of chow-fed mice at 3 ($P < 0.05$) and 4 ($P < 0.0005$) weeks of HFD feeding (Figure 2A). By 16 weeks, skeletal muscle *mkp-1* mRNA levels were approximately 3-fold higher in mice fed the HFD than in chow-fed mice ($P < 0.05$; Figure 2A). These results demonstrate that MKP-1 in skeletal muscle is a target for upregulation in response to HFD feeding.

Excess levels of FAs have been shown to induce the expression of a number of genes. We hypothesized that FAs, which constitute a major component of a HFD, might be responsible, at least in part, for inducing the upregulation of MKP-1 in skeletal muscle. Using a luciferase reporter construct containing 1.4 Kb of the MKP-1 promoter (32), we assessed the ability of multiple types of FAs to induce MKP-1 expression in C2C12 myoblasts. We found that MKP-1 transcription increased by approximately 2.5-fold in C2C12 myoblasts after exposure to the saturated FA palmitate (Figure 2B). In contrast, both the unsaturated FA palmitoleate and the omega-3 FA eicosapentaenoic acid failed to stimulate MKP-1 transcription in C2C12 myoblasts (Figure 2B). Notably, the activation of MKP-1 transcription by palmitate was comparable to that of anisomycin, an established inducing agent of MKP-1 transcription. In order to verify the luciferase results, we stimulated C2C12 myoblasts with palmitate, isolated mRNA, and performed quantitative real-time RT-PCR. We found that *mkp-1* mRNA levels increased by approximately 2-fold within 10 minutes of palmitate stimulation and remained elevated for at least 3 hours (Figure 2C). Similar results were also obtained when C2C12 myoblasts were differentiated into myotubes (data not shown).

It has been reported that palmitoleate, when added with saturated FAs chronically, can abrogate the effects of saturated FAs (27, 33, 34). In order to assess whether the unsaturated FA palmitoleate rescues the induction of MKP-1 by palmitate, we treated C2C12 myoblasts with palmitate, palmitoleate, or their combination for 30 minutes, isolated mRNA, and performed quantitative real-time RT-PCR. The

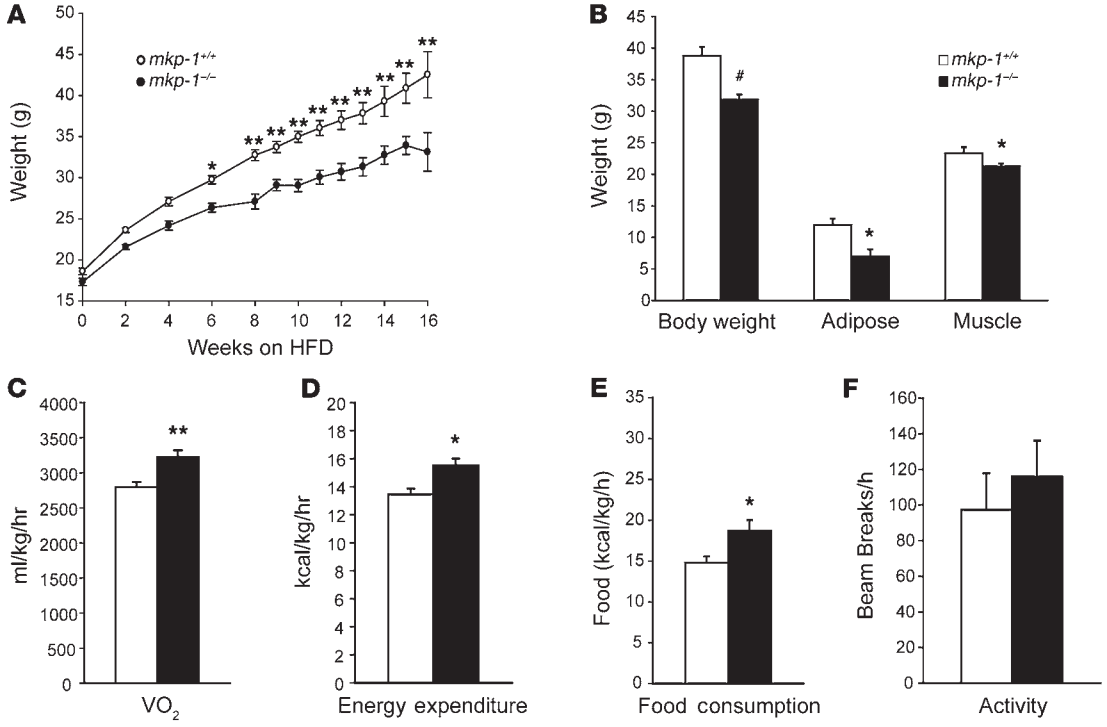

Figure 1

Resistance to diet-induced obesity and increased energy expenditure in *mkp-1*$^{-/-}$ mice. (**A**) 129/J *mkp-1*$^{+/-}$ mice were backcrossed to wild-type C57BL6/J mice for 8 generations. At weaning, backcrossed *mkp-1*$^{+/+}$ and *mkp-1*$^{-/-}$ mice were placed on a HFD, and weights were monitored weekly for 16 weeks. Data are mean ± SEM (n = 8–16 per time point). (**B**) *mkp-1*$^{+/+}$ and *mkp-1*$^{-/-}$ mice were subjected to proton magnetic resonance spectroscopy analysis after 16 weeks of HFD feeding (n = 6–8). Data are mean ± SEM. (**C**–**F**) *mkp-1*$^{+/+}$ and *mkp-1*$^{-/-}$ mice were subjected to open circuit calorimetry after 16 weeks of HFD feeding, and (**C**) oxygen consumption, (**D**) energy expenditure, (**E**) food consumption, and (**F**) locomotor activity were recorded. Data in **C**–**F** are mean ± SEM (n = 6–8). $^{*}P < 0.05$, $^{**}P < 0.005$, $^{\#}P < 0.0005$ versus *mkp-1*$^{+/+}$.

addition of palmitoleate to the lipid mixture ameliorated the induction of MKP-1 in response to palmitate (Supplemental Figure 2A). In addition, we found no evidence for changes in myoblast cytotoxicity with palmitate in the absence or presence of palmitoleate (Supplemental Figure 2B). These results make it unlikely that the increase in MKP-1 expression is caused by nonspecific actions of palmitate.

We also extended these studies to examine whether 18 carbon chain FAs, stearate and oleate, were able to induce MKP-1 expression. We found that *mkp-1* mRNA levels increased approximately 2-fold when C2C12 myoblasts were exposed for 30 minutes to either stearate or oleate (Supplemental Figure 2A). We next analyzed the content of skeletal muscle lipid metabolites in mice fed a HFD. These results indicated that total skeletal muscle lipid metabolites were significantly elevated in HFD-fed mice compared with chow-fed mice (Supplemental Figure 2C). In addition, quantitation of individual lipid metabolites revealed increases of approximately 20%–50% for palmitate, palmitoleate, stearate, and oleate in skeletal muscle of HFD mice (Supplemental Figure 2D). Collectively, these results demonstrate that multiple FAs are elevated in skeletal muscle after HFD feeding, which suggests that FAs may be responsible for the upregulation of MKP-1.

An immediate-early gene, *mkp-1* is activated in response to a variety of stresses in a MAPK-dependent manner. We speculated that one or more of the MAPKs (Erk, JNK, and/or p38 MAPK) might be responsible for mediating the effects of palmitate-induced activation of MKP-1 transcription. To test this, we inhibited the MEK/Erk, JNK, and p38 MAPK pathways by pretreating C2C12 myoblasts with the pharmacological inhibitors U0126, SP600125, and SB203580, respectively, followed by palmitate treatment. We found that U0126 and SP600125 prevented palmitate-induced expression of *mkp-1* mRNA, whereas SB203580 was without effect (Figure 2D). These results demonstrated that MKP-1 expression was induced in muscle cells by palmitate in a JNK- and Erk-dependent manner. Finally, we evaluated whether palmitate regulates MKP-1 expression at the protein level. In order to assess this, we stimulated C2C12 myoblasts with palmitate for 30 or 60 minutes and immunoblotted for MKP-1 expression. Indeed, MKP-1 protein expression was induced by palmitate in C2C12 myoblasts after 30 minutes of stimulation (Figure 2E). These results support the conclusion that in myoblasts, MKP-1 is a target for upregulation by FAs.

MKP-1 mediates oxidative myofiber loss in obesity. An excess of dietary FA intake has been associated with a loss of expression of genes that regulate oxidative myofiber composition (26). If, when overexpressed during HFD feeding, MKP-1 plays an essential role in mediating the loss of oxidative myofiber composition, then *mkp-1*$^{-/-}$ mice should be resistant to oxidative myofiber loss after HFD feeding. In order to assess this, we stained skeletal muscle sections derived from *mkp-1*$^{+/+}$ and *mkp-1*$^{-/-}$ mice for NADH dehydrogenase, succinate dehydrogenase, and cytochrome oxidase activities in order to assess skeletal muscle oxidative capacity. Skeletal muscle isolated from the tibialis anterior (TA) of *mkp-1*$^{+/+}$ mice displayed a decreased level of oxidative capacity after 16 weeks on the HFD

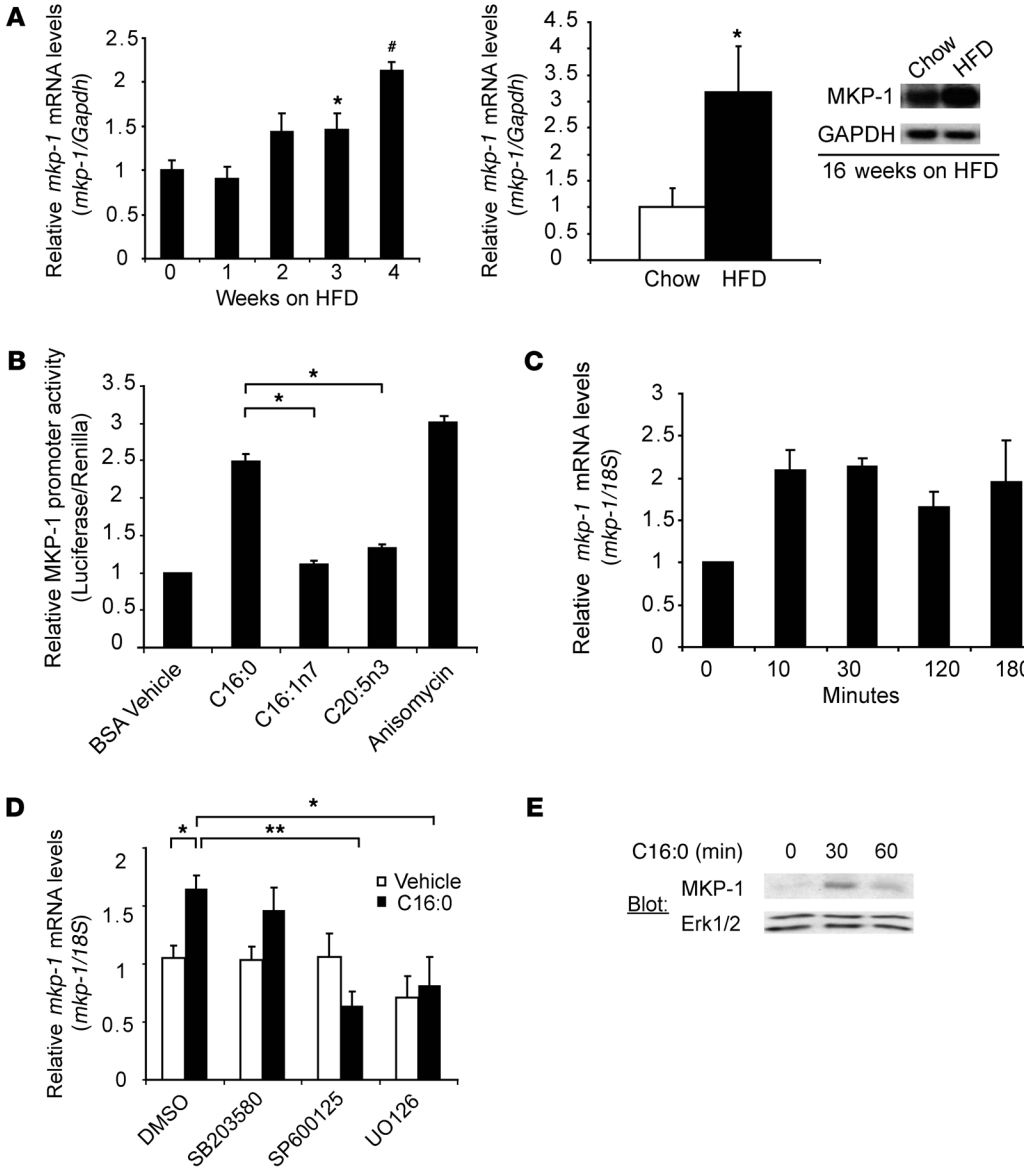

Figure 2

HFD and FAs induce MKP-1 overexpression in skeletal muscle. (**A**) Quadriceps were isolated from mice fed chow or HFD for the indicated times. Northern blots were performed for MKP-1 and normalized to GAPDH. Shown are normalized *mkp-1* mRNA levels for 0–4 weeks of HFD (n = 3–9) or for 16-week chow- or HFD-fed mice (n = 6–7). A representative Northern blot image is shown for the latter. Data are mean ± SEM. (**B**) C2C12 myoblasts were transfected with MKP-1 promoter–luciferase (–1.4 kb) and TK-Renilla and stimulated for 16 hours with 500 μM palmitate (C16:0), palmitoleate (C16:1n7), eicosapentaenoic acid (C20:5n3), and anisomycin. Data are mean ± SEM of luciferase normalized to Renilla relative to vehicle control (n = 3–7). (**C**) C2C12 myoblasts were stimulated with 500 μM palmitate for the indicated times, RNA was harvested, and *mkp-1* mRNA levels were measured by quantitative real-time RT-PCR and normalized to *18S*. Data are mean ± SEM from 3–7 experiments. (**D**) C2C12 myoblasts were pretreated with the indicated MAPK inhibitors and stimulated with vehicle or 500 μM palmitate for 30 minutes. MKP-1 levels were determined as in **C**. Data are mean ± SEM from 3–7 experiments. (**E**) C2C12 myoblasts were stimulated for the indicated times with 500 μM palmitate and immunoblotted for MKP-1 or Erk1/2. Immunoblot is representative of 3 separate experiments. $^{*}P < 0.05$, $^{**}P < 0.005$, $^{\#}P < 0.0005$ versus respective control or as otherwise indicated by brackets.

compared with chow-fed *mkp-1*$^{+/+}$ mice (Figure 3, A–C). In contrast, *mkp-1*$^{-/-}$ mice did not show decreased oxidative myofiber content when fed a HFD compared with chow-fed *mkp-1*$^{-/-}$ mice. Moreover, HFD-fed *mkp-1*$^{-/-}$ mice expressed significantly higher levels of oxidative myofibers than did HFD-fed *mkp-1*$^{+/+}$ mice ($P < 0.05$; Figure 3, A–C). Hence, MKP-1 is involved in promoting the loss of oxidative myofiber composition during HFD feeding.

Adult skeletal muscle composition is relatively heterogeneous; however, certain muscle groups are enriched in particular myofibers. The soleus is highly oxidative, whereas the quadriceps contains mostly glycolytic myofibers. The composition of these myofibers is determined by the expression of myofibrillar proteins called myosin heavy chains (MHCs), of which there are 4 types in adult skeletal muscle: MHCI, MHCIIA, MHCIIX, and MHCIIB. MHCI is the most

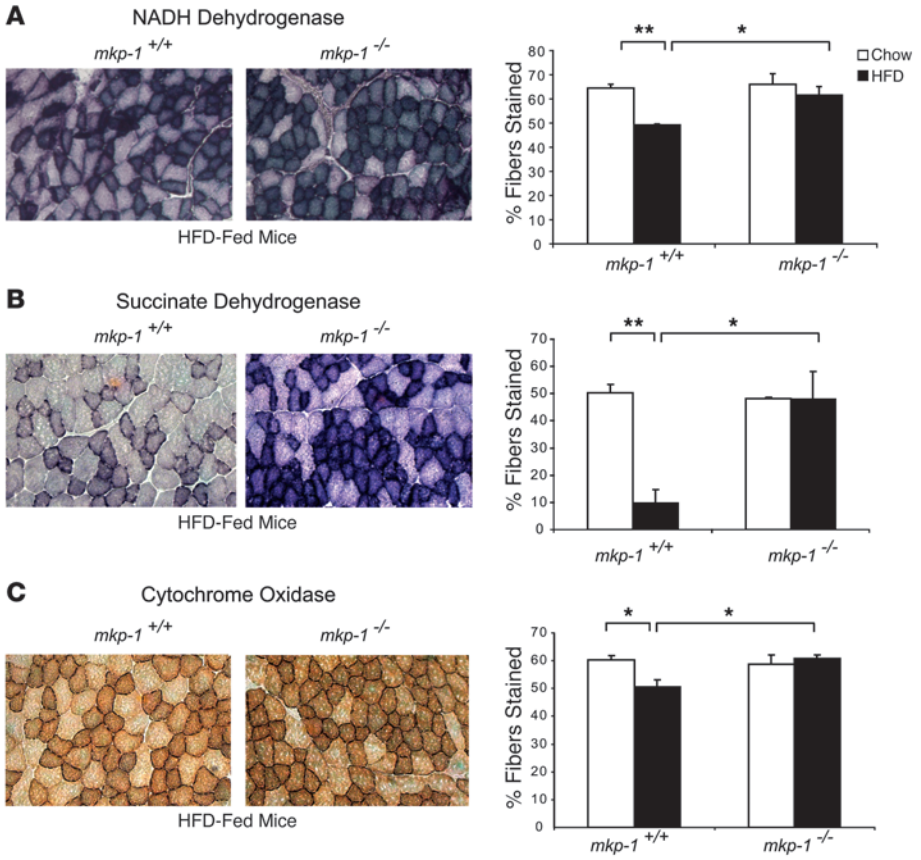

Figure 3
MKP-1 mediates oxidative myofiber loss in obesity. (**A**) NADH dehydrogenase stain and quantitation (n = 5–6) of TA muscle from HFD-fed *mkp-1*$^{+/+}$ and *mkp-1*$^{-/-}$ mice. (**B**) Succinate dehydrogenase stain and quantitation (n = 3) of TA muscle from HFD-fed *mkp-1*$^{+/+}$ and *mkp-1*$^{-/-}$ mice. (**C**) Cytochrome oxidase stain and quantitation (n = 3–5) of TA muscle from HFD-fed *mkp-1*$^{+/+}$ and *mkp-1*$^{-/-}$ mice. Original magnification, ×100. Data are mean ± SEM. *P < 0.05; **P < 0.005.

oxidative myofiber, whereas MHCIIB is the most glycolytic. MHCIIA and MHCIIX are intermediate myofibers of higher oxidative capacity than MHCIIB (15). We performed immunohistochemistry for all 4 MHC types in *mkp-1*$^{+/+}$ and *mkp-1*$^{-/-}$ mice after 16 weeks on a HFD (Figure 4, A and B). We observed a trend toward increased expression levels of the oxidative MHCI and a significantly increased percentage of MHCIIA in *mkp-1*$^{-/-}$ mice compared with *mkp-1*$^{+/+}$ mice after 16 weeks on a HFD (P < 0.05; Figure 4B). Increased levels of MHCIIX were observed in *mkp-1*$^{-/-}$ mice compared with *mkp-1*$^{+/+}$ mice fed a chow diet. We noted increased percentages of MHCIIB myofibers in HFD-fed *mkp-1*$^{+/+}$ mice, although *mkp-1*$^{-/-}$ mice failed to exhibit increased levels of MHCIIB after HFD feeding (Figure 4B). These results demonstrate that HFD-fed *mkp-1*$^{-/-}$ mice maintained a higher oxidative capacity in skeletal muscle and were resistant to a HFD-induced switch to glycolytic myofibers.

MKP-1 negatively regulates PGC-1α function. The enhanced oxidative myofiber composition of *mkp-1*$^{-/-}$ mice after HFD feeding (Figures 3 and 4) suggests that MKP-1 negatively regulates oxidative myofiber composition. To explore the mechanisms underlying this response, we sought a molecular target through which the actions of MKP-1 could exert an effect on skeletal muscle oxidative capacity. One such target is PGC-1α, a transcriptional coactivator that plays an important role in both promotion and maintenance of skeletal muscle oxidative capacity (20). mRNA expression, coactivator activity, and protein stability of PGC-1α have all been reported to be positively regulated by p38 MAPK (27, 29, 30, 35, 36). Because MKP-1 negatively regulates p38 MAPK activity in skeletal muscle (14), we hypothesized that HFD-induced MKP-1 overexpression antagonizes p38 MAPK–mediated PGC-1α function. PGC-1α activity increases in response to cytokine stimulation in a p38 MAPK–dependent manner, in part due to relief of binding of negative regulators of transcription, such as the histone deacetylase p160^{MBP} (29, 30, 35, 36). In order to determine whether MKP-1 negatively regulates PGC-1α activity, we used a chimera encoding full-length PGC-1α and the DNA-binding domain of GAL4. In response to TNF-α, PGC-1α activity was induced by approximately 2-fold (Figure 5A). Upon overexpression of MKP-1, PGC-1α activity decreased in a dose-dependent manner both basally and in response to TNF-α stimulation (Figure 5A). siRNA knockdown experiments were performed to test whether MKP-1 is essential for the negative regulation of PGC-1α activity. Knockdown of MKP-1 using siRNA resulted in a 70% decrease in *mkp-1* mRNA levels (data not shown) and an approximately 90% decrease in MKP-1 protein expression (Figure 5B). In C2C12 myoblasts in which MKP-1 had been knocked down, we observed an enhanced level of PGC-1α activity both basally and in response to TNF-α stimulation compared with nontargeting siRNA–treated myoblasts (Figure 5B). These results demonstrate that MKP-1 plays an essential role in attenuating PGC-1α activity.

To test whether MKP-1 affects PGC-1α at the transcriptional level, we used a reporter containing the PGC-1α promoter (–2.0 kb) fused to luciferase and transfected this into C2C12 myoblasts in the presence or absence of MKP-1. Overexpression of MKP-1 decreased PGC-1α transcription more than 3-fold (Figure 5C). Moreover, when p38 MAPK activation was stimulated by expressing a constitutively active mutant of MKK6, overexpression of MKP-1 was also capable of suppressing PGC-1α transcription. These results indicate that MKP-1 can negatively regulate PGC-1α transcription. To substantiate the observation that MKP-1 overexpression attenuates PGC-1α transcription, we measured *Ppargc1a* mRNA levels in skeletal muscle of *mkp-1*$^{+/+}$ and *mkp-1*$^{-/-}$ mice fed chow or HFD. Although chow-fed *mkp-1*$^{-/-}$ mice displayed a 2-fold increase in *Ppargc1a* mRNA levels in the TA compared with chow-fed *mkp-1*$^{+/+}$ mice (P < 0.05), *mkp-1*$^{+/+}$ and *mkp-1*$^{-/-}$ mice surprisingly displayed equivalent levels of *Ppargc1a* mRNA after HFD feeding (Figure 5D). These data raised the possibility that during HFD feeding, MKP-1 might regulate PGC-1α function through a posttranslational mechanism.

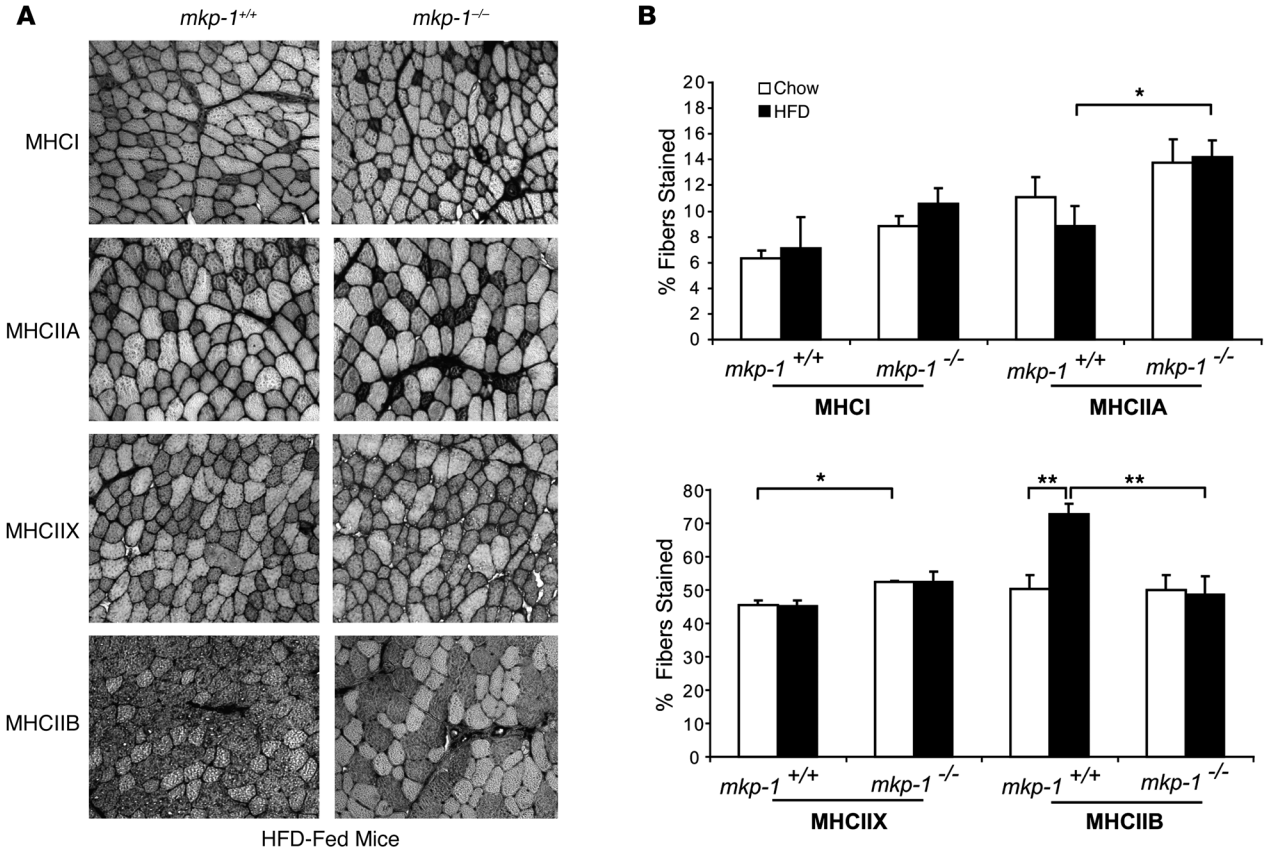

Figure 4
MKP-1 mediates a glycolytic fiber type switch in obesity. (**A**) Photomicrographs representing MHCI, MHCIIA, MHCIIX, and MHCIIB immunohistochemical staining of TA muscle from HFD-fed *mkp-1*$^{+/+}$ and *mkp-1*$^{-/-}$ mice. Original magnification, ×100. (**B**) Percentage of fiber type stained (n = 4–8). Data are mean ± SEM. *P < 0.05; **P < 0.005.

MKP-1 attenuates PGC-1α function by suppressing PGC-1α stability. Our results showed that MKP-1 did not affect *Ppargc1a* mRNA levels after HFD feeding (Figure 5D).We speculated that MKP-1 may affect PGC-1α protein expression through a p38 MAPK–dependent pathway (29, 35). An attractive hypothesis was that MKP-1 negatively regulates PGC-1α stability by indirectly controlling its phosphorylation. To test this, PGC-1α was transiently expressed in C2C12 myoblasts in combination with activated MKK6 or MKK7 in order to constitutively activate p38 MAPK and JNK, respectively. Consistent with previous observations (29), activation of p38 MAPK, but not JNK (or Erk; data not shown), increased the accumulation of PGC-1α in C2C12 myoblasts (Figure 6A). As expected, overexpression of MKP-1 antagonized phosphorylation of both p38 MAPK and JNK. PGC-1α accumulation was inhibited upon overexpression of MKP-1 in myoblasts, both under basal conditions and when coexpressed with MKK6 or MKK7 (Figure 6A). Because p38 MAPK, but neither JNK nor Erk, promoted PGC-1α stability, these results imply that when overexpressed, MKP-1 prevented the accumulation of PGC-1α by impairing p38 MAPK activity. In order to assess whether MKP-1 is essential for the regulation of PGC-1α stability, we knocked down MKP-1 in C2C12 myoblasts and performed pulse-chase experiments to measure $t_{1/2}$ of PGC-1α. Loss of MKP-1 increased PGC-1α $t_{1/2}$ by 47% compared with nontargeting siRNA–treated myoblasts (P < 0.05; Figure 6B). These results demonstrate that MKP-1 negatively regulates PGC-1α stability.

MKP-1 regulates p38 MAPK–dependent phosphorylation of PGC-1α. p38 MAPK phosphorylates PGC-1α on 3 sites, Thr262, Ser265, and Thr298, resulting in its increased protein stability (29). Of the MAPKs, only p38 MAPK is capable of promoting PGC-1α stability, which indicates that MKP-1 must act through p38 MAPK to antagonize PGC-1α phosphorylation and hence stability. In order to directly establish whether MKP-1 inactivates p38 MAPK–mediated phosphorylation of PGC-1α, we generated PGC-1α phospho-specific antibodies to phospho-Ser265 and phospho-Thr298. When PGC-1α was coexpressed with activated MKK6, antibodies to both phospho-Ser265 and phospho-Thr298 on PGC-1α detected phosphorylated PGC-1α (Figure 6C). Importantly, when Ser265 or Thr298 on PGC-1α was mutated to nonphosphorylatable alanine residues and overexpressed with activated MKK6 in C2C12 myoblasts, antibodies to phospho-Ser265 and phospho-Thr298 PGC-1α barely detected phosphorylated PGC-1α at either residue (Figure 6C). These results demonstrate the specificity of these antibodies to phospho-Ser265 and phospho-Thr298 on PGC-1α.

We next determined whether MKP-1 overexpression impairs p38 MAPK-mediated PGC-1α phosphorylation. In order to assess the effects of MKP-1 on PGC-1α phosphorylation independently of its effects on PGC-1α stability, we established an expression level of MKP-1 that did not dramatically affect the accumulation of PGC-1α, as observed in previous experiments (Figure 6A). We induced phosphorylation of PGC-1α in C2C12 myoblasts by expressing

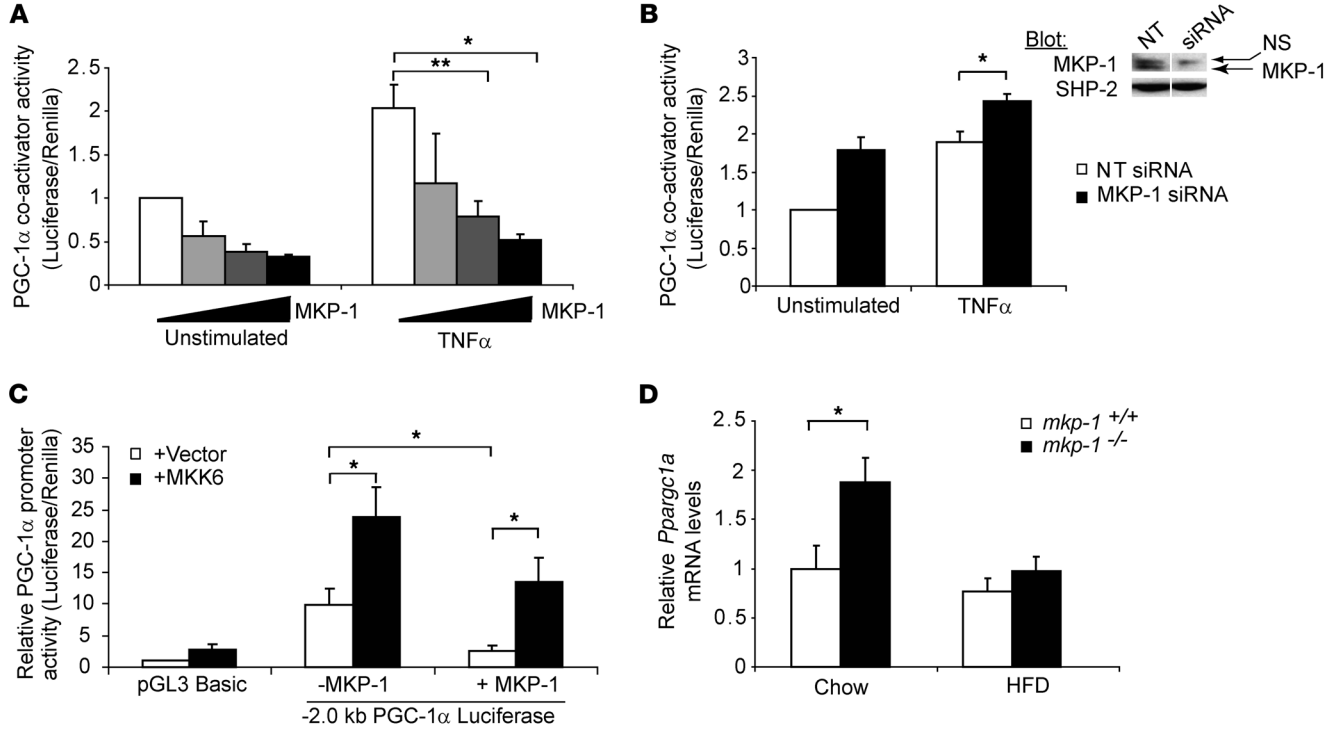

Figure 5

MKP-1 negatively regulates PGC-1α coactivator activity. (**A**) PGC-1α–GAL4, 5xGAL4-luciferase, increasing concentrations of MKP-1, and TK-Renilla were transfected into C2C12 myoblasts. Myoblasts were stimulated with 10 ng/ml TNF-α for 24 hours prior to measurement of luciferase and Renilla. Data are mean ± SEM normalized luciferase/Renilla values from 4 separate experiments. (**B**) Left: PGC-1α–GAL4, 5xGAL4-luciferase, and TK-Renilla were transfected into C2C12 myoblasts along with 50 nM MKP-1 or nontargeting (NT) siRNA. Myoblasts were starved and either left unstimulated or stimulated with 10 ng/ml TNF-α for 24 hours prior to measurement of luciferase and Renilla. Data are mean ± SEM normalized luciferase/Renilla from 3 separate experiments. Right: C2C12 myoblasts were transfected with 50 nM of either MKP-1 or nontargeting siRNA; 24 hours later, cells were immunoblotted for MKP-1 or SHP-2 as a loading control. Lanes were run on the same gel but were noncontiguous (white line). (**C**) pGL3-PGC-1α promoter–luciferase (–2.0 kb) and TK-Renilla were transfected into C2C12 myoblasts in the absence or presence of MKP-1 and MKK6EE. Luciferase and Renilla were measured 48 hours later. Data are mean ± SEM normalized luciferase/Renilla values from 4 separate experiments. (**D**) *Ppargc1a* mRNA levels in TA muscle of age-matched *mkp-1*$^{+/+}$ and *mkp-1*$^{-/-}$ mice after 16 weeks of chow or HFD, as measured by quantitative real-time RT-PCR. Data are mean ± SEM normalized to *18S* mRNA (n = 5–8). *P < 0.05; **P < 0.005.

activated MKK6 in the absence or presence of MKP-1. Under these conditions, MKP-1 overexpression reduced PGC-1α phosphorylation on both Ser265 and Thr298 by approximately 50% (Figure 6D). Therefore, overexpression of MKP-1 impaired PGC-1α phosphorylation at sites that directly promote its stability.

Next we determined whether MKP-1 is required for regulating inducible phosphorylation on PGC-1α through activation of endogenous signaling pathways in myoblasts. MKP-1 was knocked down in C2C12 myoblasts by transfection with MKP-1 siRNA or with nontargeting siRNA as a control. These myoblasts were stimulated with TNF-α and IL-1β for various times. Immunoblotting of Flag-tagged PGC-1α immunoprecipitates prepared from nontargeting and MKP-1 siRNA–targeted myoblasts revealed that knockdown of MKP-1 resulted in increased basal levels of PGC-1α phosphorylation at both phospho-Ser265 and phospho-Thr298 (Figure 6E). After stimulation with TNF-α and IL-1β, nontargeting siRNA–treated myoblasts exhibited increased levels of phospho–PGC-1α at Ser265 and, to a lesser extent, Thr298. However, MKP-1 siRNA–treated myoblasts showed a pronounced enhancement in the levels of phospho–PGC-1α at Ser265 and Thr298 compared with nontargeting siRNA–treated myoblasts. Concomitantly, increased PGC-1α expression was observed both basally and in response to stimulation with TNF-α and IL-1β in MKP-1 siRNA–treated myoblasts compared with nontargeting siRNA–treated myoblasts (Figure 6E).

Our observations in myoblasts demonstrated that MKP-1 overexpression antagonized p38 MAPK–mediated phosphorylation of PGC-1α (Figure 6). We therefore asked whether the increased MKP-1 observed after HFD feeding (Figure 2) impairs p38 MAPK–mediated PGC-1α phosphorylation and leads to reduced PGC-1α expression levels in skeletal muscle. MKP-1 is localized to the nucleus, and we previously showed that MKP-1 plays a major role in dephosphorylating the nuclear pool of JNK in vivo (14). Therefore, we assessed whether the nuclear pool of p38 MAPK activity is attenuated in mice fed a HFD. We prepared nuclear extracts from TA muscle (Supplemental Figure 3A) and immunoblotted the extracts for phosphorylated p38 MAPK. We noted no difference in nuclear p38 MAPK phosphorylation between *mkp-1*$^{+/+}$ and *mkp-1*$^{-/-}$ mice fed a chow diet (Figure 7A). However, there was a 35% decrease in p38 MAPK phosphorylation in the nucleus of *mkp-1*$^{+/+}$ mice fed the HFD compared with chow-fed *mkp-1*$^{+/+}$ mice. Moreover, there was a significant increase in p38 MAPK phosphorylation in nuclear extracts derived from *mkp-1*$^{-/-}$ mice compared with *mkp-1*$^{+/+}$ mice fed the HFD (P = 0.05; Figure 7A). Because mice lacking MKP-1

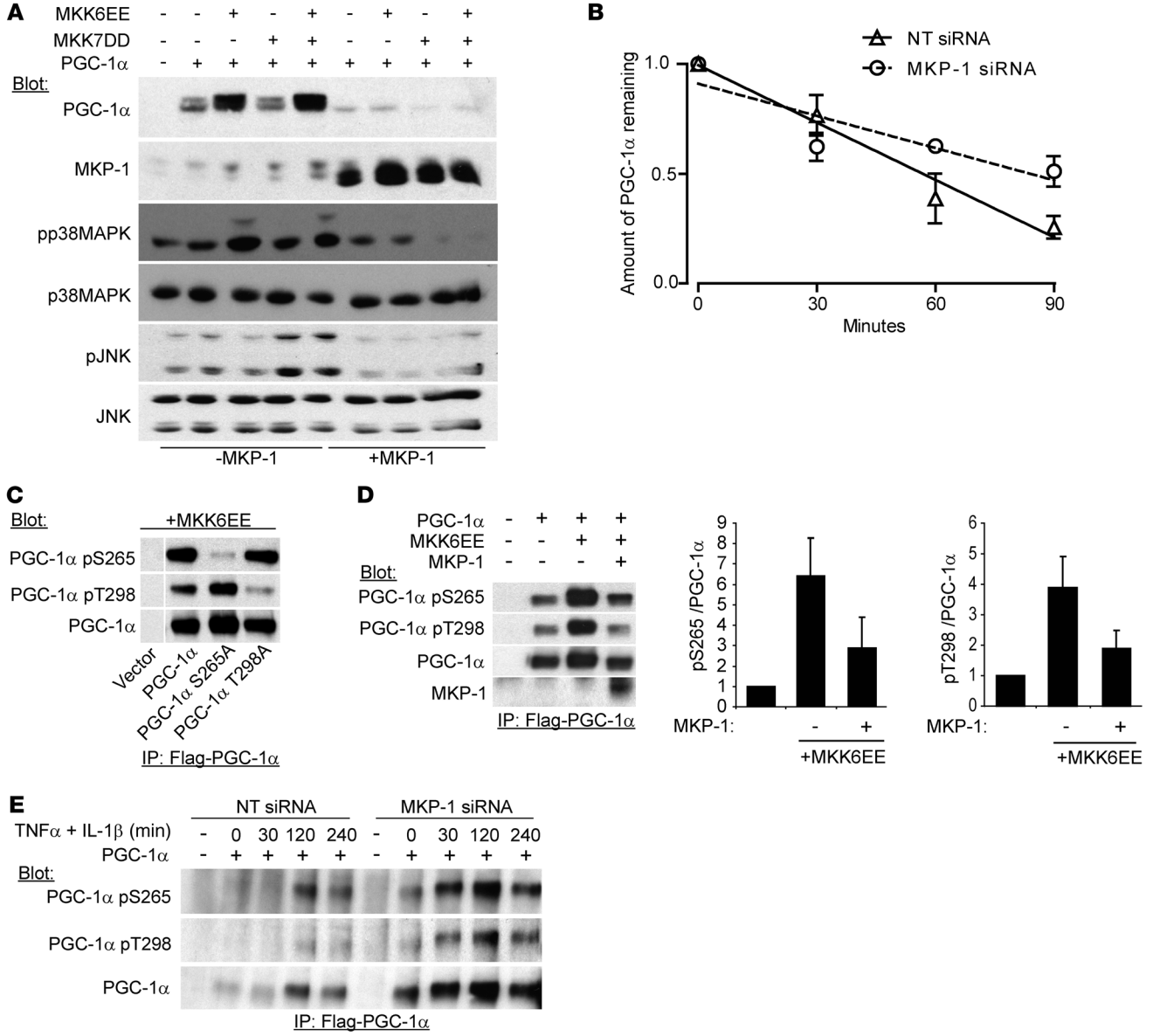

Figure 6

MKP-1 antagonizes PGC-1α phosphorylation and protein stability. (**A**) Flag-tagged PGC-1α, MKK6EE, MKK7DD, and MKP-1 (10 μg) were transfected into C2C12 myoblasts. Myoblasts were lysed 24 hours later and immunoblotted with PGC-1α, MKP-1, phospho-p38 MAPK, p38 MAPK, phospho-JNK, and JNK antibodies. (**B**) Flag-tagged PGC-1α was transfected into C2C12 myoblasts along with nontargeting siRNA or MKP-1 siRNA as described in Figure 5B, and pulse-chase metabolic labeling with ^{35}S methionine/cysteine was performed. Densitometric analyses were quantitated as the amount of PGC-1α remaining relative to time 0. The mean $t_{1/2}$ was calculated from the linear regression derived from 3 independent experiments (nontargeting siRNA, 56.7 minutes; MKP-1 siRNA, 83.5 minutes; $P < 0.05$). Data are mean ± SEM. (**C**) Flag-tagged PGC-1α as well as Flag-tagged PGC-1α Ser265A and Thr298A mutants were transfected into C2C12 myoblasts with MKK6EE. Myoblasts were lysed, and PGC-1α was immunoprecipitated with anti-Flag antibodies and immunoblotted with total PGC-1α, phospho-Ser265 PGC-1α, or phospho-Thr298 PGC-1α antibodies. Lanes were run on the same gel but were noncontiguous (white line). (**D**) Flag-PGC-1α, MKK6EE, and MKP-1 (2 μg) were transfected into C2C12 myoblasts. Myoblasts were lysed, and PGC-1α was immunoprecipitated with anti-Flag antibodies and immunoblotted as in **C**. Graphs show densitometric measurements of phospho-Ser265 PGC-1α and phospho-Thr298 PGC-1α normalized to total PGC-1α from 3 independent experiments. Data are mean ± SEM. (**E**) Flag-tagged PGC-1α was transfected into C2C12 myoblasts along with 50 nM nontargeting or MKP-1 siRNA. Myoblasts were starved for 2 hours prior to stimulation with 10 ng/ml TNF-α and 2 ng/ml IL-1β for the indicated times. Myoblasts were lysed, and PGC-1α was immunoprecipitated with anti-Flag antibodies and immunoblotted as in **C**.

exhibited not a decreased, but rather an enhanced, level of p38 MAPK activity after HFD feeding, these results collectively imply that MKP-1 overexpression induced by HFD feeding promotes nuclear p38 MAPK inactivation in skeletal muscle.

Based on these results and those presented in Figure 6, we anticipated that the phosphorylation and, hence, expression levels of PGC-1α would be greater in skeletal muscle of *mkp-1*$^{-/-}$ mice after HFD feeding. We prepared nuclear extracts from TA muscle (Sup-

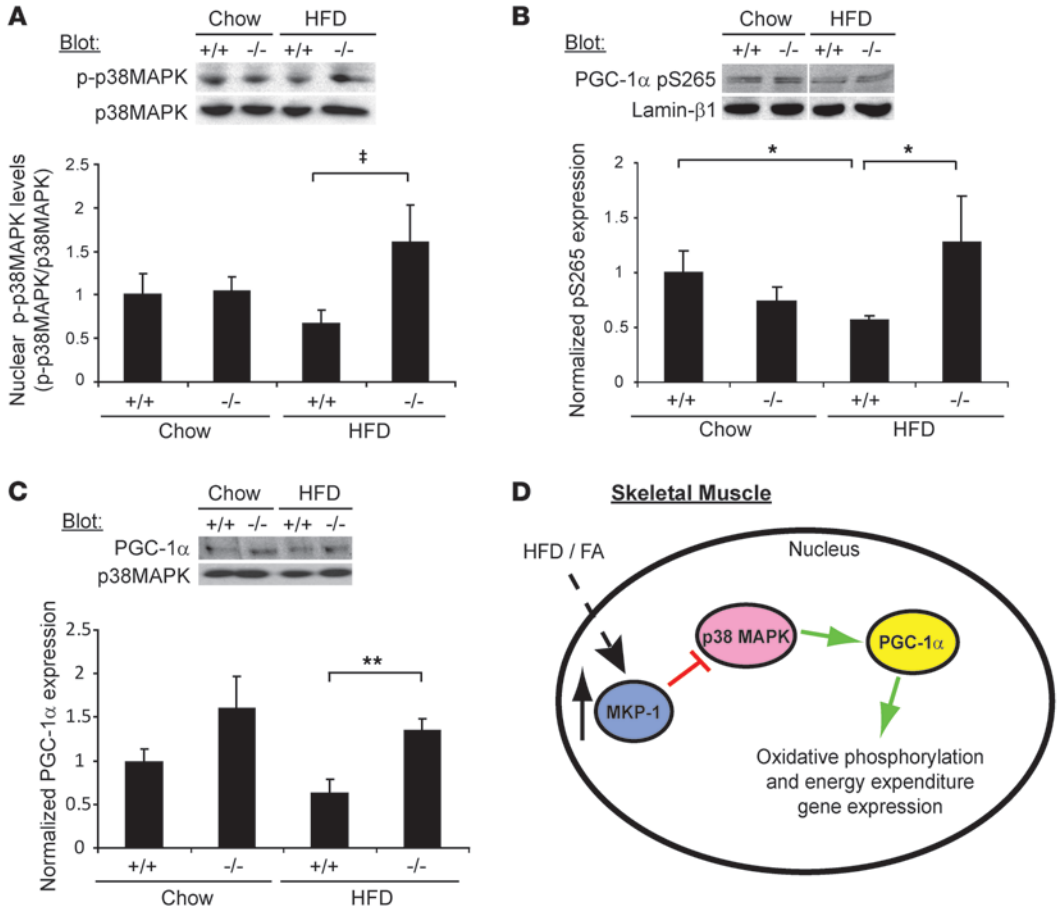

Figure 7

Enhanced PGC-1α expression and phosphorylation in *mkp-1*$^{-/-}$ mice. (**A**) Nuclear extracts of TA muscle from age-matched *mkp-1*$^{+/+}$ and *mkp-1*$^{-/-}$ mice fed chow or HFD for 16 weeks were immunoblotted for phospho–p38 MAPK or p38 MAPK. Also shown are densitometric measurements for phospho–p38 MAPK levels normalized to total p38 MAPK. Data are mean ± SEM (n = 8–9). (**B**) Nuclear extracts as in **A** were immunoblotted for phospho-Ser265 PGC-1α. Lanes were run on the same gel but were noncontiguous (white line). Also shown are densitometric measurements for phospho-Ser265 PGC-1α expression normalized to Lamin-β1. Data are mean ± SEM (n = 4–9). (**C**) TA muscle was isolated from *mkp-1*$^{+/+}$ and *mkp-1*$^{-/-}$ mice fed chow or HFD for 16 weeks. Muscle lysates were immunoblotted with PGC-1α antibodies, and densitometric measurements for PGC-1α expression were normalized to p38 MAPK. Data are mean ± SEM (n = 6). (**D**) Under HFD conditions, exposure to FAs increases MKP-1 expression, causing inactivation of nuclear p38 MAPK. Reduced p38 MAPK–mediated phosphorylation of PGC-1α decreases PGC-1α expression. Impaired skeletal muscle PGC-1α function facilitates loss of oxidative myofiber composition. ‡P = 0.05; *P < 0.05; **P < 0.005.

plemental Figure 3A) and immunoblotted for phospho-Ser265 PGC-1α. Although no differences in phospho-Ser265 PGC-1α levels were found in *mkp-1*$^{+/+}$ or *mkp-1*$^{-/-}$ mice fed a chow diet, we noted a significant decrease in the level of phospho-Ser265 PGC-1α in HFD-fed compared with chow-fed *mkp-1*$^{+/+}$ mice (P < 0.05; Figure 7B). Furthermore, the levels of phospho-Ser265 PGC-1α in HFD-fed *mkp-1*$^{-/-}$ mice were significantly greater than those of HFD-fed *mkp-1*$^{+/+}$ mice (P < 0.05; Figure 7B). Next, we isolated TA muscle from *mkp-1*$^{+/+}$ and *mkp-1*$^{-/-}$ mice after chow or HFD feeding and performed immunoblots for the expression of PGC-1α. PGC-1α levels decreased after HFD feeding in *mkp-1*$^{+/+}$ mice, whereas on the chow diet, PGC-1α levels in *mkp-1*$^{-/-}$ mice were elevated compared with *mkp-1*$^{+/+}$ mice (Figure 7C). This is likely because of the elevated levels of *Ppargc1a* mRNA in chow-fed mice (Figure 5D). Remarkably, although there were equivalent levels of *Ppargc1a* mRNA in *mkp-1*$^{+/+}$ and *mkp-1*$^{-/-}$ mice after HFD feeding (Figure 5D), the levels of PGC-1α protein were significantly elevated in *mkp-1*$^{-/-}$ mice compared with *mkp-1*$^{+/+}$ mice (P < 0.05; Figure 7C). These results are consistent with the enhanced phosphorylation on p38 MAPK–dependent sites that increase PGC-1α stability. Together, these data demonstrated that MKP-1, via negative regulation of p38 MAPK–dependent phosphorylation of PGC-1α, plays an essential role in attenuating PGC-1α expression in HFD-fed mice.

Discussion

In this report, we show that MKP-1 plays an important role in the regulation of oxidative myofiber composition. Several groups have found that in obese individuals, the composition of oxidative myofibers is reduced and the expression levels of glycolytic myofibers are increased (37–39). The consequences of oxidative myofiber loss may represent one of the many pathologic sequelae that accompany obesity. Our results suggest that MKP-1 plays a role in facilitating the loss of oxidative myofibers in obesity. We

identify PGC-1α as a candidate through which MKP-1 interfaces, by negative regulation of p38 MAPK, to link changes in metabolic status to oxidative myofiber composition.

Our results demonstrate a requirement for MKP-1 in the control of metabolic homeostasis (Figure 1). However, the mechanistic basis for how MKP-1 is involved in metabolic signaling, and whether MKP-1 plays a role in metabolic dysfunction, remains unanswered. We addressed these questions by establishing whether the expression levels of MKP-1 were altered in response to HFD feeding in mice. After the onset of HFD feeding, the MKP-1 expression increased and remained elevated throughout the entire course of the HFD (Figure 2A). Likewise, the activity of p38 MAPK, a substrate of MKP-1, decreased in the nucleus of skeletal muscle derived from *mkp-1*$^{+/+}$ mice after HFD feeding and was enhanced in *mkp-1*$^{-/-}$ mice (Figure 7A). Hence, as previously reported (14), MKP-1 serves as an essential negative regulator of the nuclear pool of MAPKs.

Numerous stimuli and stresses have been shown to induce the expression of *mkp-1*. We were particularly interested in whether MKP-1 expression is responsive to changes in nutrients that constitute components of a HFD. The results of our experiments demonstrated that exposure of myoblasts to FAs upregulated *mkp-1* mRNA levels (Figure 2, B and C, and Supplemental Figure 2A). MKP-1 was rapidly responsive to palmitate, stearate, and oleate, but not to palmitoleate or eicosapentaenoic acid, which suggests that its upregulation is coupled to a precise signaling pathway rather than a nonspecific consequence of increases in FA load and/or cytotoxicity (Supplemental Figure 2B). In this regard, we found that Erk and JNK, but not p38 MAPK, mediated palmitate-induced upregulation of MKP-1 (Figure 2D). Provocatively, FAs are capable of stimulating the TLR4 pathway (34), and we have previously shown that MKP-1 is upregulated in response to engagement of the TLR4/Myd88 complex (40). Therefore, it is conceivable that in skeletal muscle, excess levels of FAs activate TLR4 signaling and cause upregulation of MKP-1. However, given the milieu of stresses to which MKP-1 expression responds, it is likely that other contributing factors participate in its activation in skeletal muscle in response to HFD feeding.

Skeletal muscle fiber composition is plastic and adapts in response to environmental and nutrient stresses. Obesity and insulin resistance have been proposed to be associated with aberrant regulation of muscle fiber specification, and obese individuals have been reported to exhibit decreased oxidative and increased glycolytic myofibers (18, 19). Nonetheless, the effects of a HFD on mitochondrial function in skeletal muscle remain somewhat controversial. Although multiple groups have shown that prolonged exposure to a HFD leads to mitochondrial dysfunction, others have found that a HFD actually leads to enhanced mitochondrial function and FA oxidation (41–43). One study has reconciled both findings by determining that a HFD increases mitochondrial efficiency in the short term (i.e., 4 weeks), but after prolonged HFD feeding (i.e., 16 weeks), the mitochondria become dysfunctional as a result of enhanced reactive oxygen species production by increased mitochondrial oxidative phosphorylation (44). We have demonstrated that *mkp-1*$^{+/+}$ mice displayed reduced skeletal muscle oxidative capacity after HFD by measurement of activities of several enzymatic components involved in mitochondrial oxidative phosphorylation (Figure 3). Furthermore, HFD-fed *mkp-1*$^{-/-}$ mice retained a high level of oxidative myofiber composition compared with HFD-fed *mkp-1*$^{+/+}$ mice (Figure 3). Oxidative MHCIIA myofibers decreased in *mkp-1*$^{+/+}$ mice after HFD feeding, whereas *mkp-1*$^{-/-}$ mice exhibited higher levels of MHCIIA myofibers basally, and the levels of these myofibers were refractory to diet-induced obesity (Figure 4). Even more striking was that *mkp-1*$^{-/-}$ mice failed to acquire increased levels of the glycolytic MHCIIB myofibers; in contrast, *mkp-1*$^{+/+}$ mice showed significantly elevated levels of MHCIIB myofibers after HFD feeding (Figure 4). These effects imply that MKP-1 overexpression negatively regulates oxidative myofiber composition and/or promotes the acquisition of glycolytic myofibers, the latter being a state represented in obesity. These data are consistent with our previous findings that skeletal muscle mitochondrial oxygen consumption is enhanced in *mkp-1*$^{-/-}$ mice (14). Previous reports have demonstrated that skeletal muscle uncoupling protein–3 (*Ucp3*) transgenic mice are resistant to diet-induced obesity as a result of increased energy expenditure (45). Indeed, *Ucp3* is a PGC-1α–responsive gene (46), and, consistent with this, MKP-1–deficient mice express increased UCP-3 levels in skeletal muscle (14). Hence, a plausible mechanism through which MKP-1–deficient mice exhibit increased energy expenditure, and subsequently resistance to diet-induced obesity, could occur through enhanced p38 MAPK–mediated activation of PGC-1α leading to increased skeletal muscle UCP-3 expression. Our previous results and those reported here are consistent with this interpretation and argue for a role for MKP-1 in negatively regulating energy expenditure. Moreover, these results support the notion that the resistance of *mkp-1*$^{-/-}$ mice to diet-induced obesity is caused, at least in part, by their ability to maintain their skeletal muscle oxidative capacity in response to HFD feeding.

A major finding of this work is the link between MKP-1 and regulation of PGC-1α. Our data show that MKP-1 overexpression inhibited PGC-1α activity in myoblasts in response to TNF-α (Figure 5A), which implies that MKP-1 antagonizes PGC-1α activity in a MAPK-dependent manner. MKP-1 also plays an essential role in the regulation of PGC-1α, since knockdown of MKP-1 expression enhanced PGC-1α activity (Figure 5B). The fact that there are 10 other MKPs, 4 of which reside in the nucleus, suggests that MKP-1 is a major nuclear-resident MKP that links MAPK signaling to PGC-1α function. We also showed that MKP-1 negatively regulated PGC-1α transcription (Figure 5C). Consistent with this, chow-fed *mkp-1*$^{-/-}$ mice expressed increased levels of *Ppargc1a* mRNA; however, this difference in mRNA was not observed in HFD-fed *mkp-1*$^{-/-}$ mice (Figure 5D). These results suggest that MKP-1 may differentially regulate PGC-1α transcription, and hence function, in a manner dependent upon nutritional status. Along these lines, although we observed increased levels of PGC-1α in chow-fed *mkp-1*$^{-/-}$ mice as a result of enhanced transcriptional activity, these expression levels are probably not themselves sufficient to increase the composition of oxidative myofibers, since much higher levels of PGC-1α appear to be required to observe such changes (22). These results suggest that the effects of MKP-1 on PGC-1α, and subsequently oxidative myofiber composition, manifest under pathophysiological conditions when mice are fed a HFD. These observations generally support the nature of *mkp-1* functioning as a stress-responsive gene.

At the posttranslational level, PGC-1α has previously been shown to be regulated by p38 MAPK (29, 35), by AMP kinase (47), and by Akt phosphorylation (48), acetylation (49), and methylation (50). Posttranslational regulation of PGC-1α by the MAPKs occurs exclusively through p38 MAPK, since neither JNK nor Erk is capable of phosphorylating PGC-1α (29). Phosphorylation of PGC-1α by p38 MAPK stimulates its activity by displacing $p160^{MBP}$, a histone deacetylase that negatively regulates PGC-1α (35). In addition, p38 MAPK phosphorylates PGC-1α, resulting in an increase in its protein stability and activity (29). Our data show that overexpression of MKP-1 dramatically impaired the steady-state expression levels of PGC-1α

and that knockdown of MKP-1 increased PGC-1α $t_{1/2}$ (Figure 6, A and B). We provide several lines of evidence that MKP-1 is a major MKP that regulates p38 MAPK–mediated control of PGC-1α phosphorylation. First, using phospho-specific antibodies directed to 2 of the 3 p38 MAPK phosphorylation sites on PGC-1α, we showed that MKP-1 overexpression inhibited PGC-1α phosphorylation at both Ser265 and Thr298 (Figure 6D). Second, loss of MKP-1 in muscle cells enhanced phosphorylation of PGC-1α on Ser265 and Thr298 and concomitantly enhanced the expression levels of PGC-1α protein (Figure 6E). Third, in HFD-fed *mkp-1*$^{-/-}$ mice, in which *Ppargc1a* mRNA levels were equivalent to those of *mkp-1*$^{+/+}$ mice (Figure 5D), PGC-1α protein levels significantly increased (Figure 7C). Finally, in HFD-fed *mkp-1*$^{+/+}$ mice, MKP-1 overexpression reduced phosphorylation of PGC-1α on Ser265, whereas HFD-fed *mkp-1*$^{-/-}$ mice did not have reduced levels of phospho-Ser265 (Figure 7B). Neither the activation of JNK (Figure 6A) nor Erk (data not shown) affected PGC-1α stability, thus eliminating these MAPKs as functionally relevant in the promotion of PGC-1α stability. In contrast, the role of p38 MAPK in the regulation of PGC-1α stability is clear. It has also been proposed that phosphorylation of Thr262 and Ser265 on PGC-1α overlies a PEST-like motif that could disrupt ubiquitination when phosphorylated (51). Collectively, these results point to the conclusion that MKP-1 controls p38 MAPK–dependent phosphorylation of PGC-1α and, hence, activity and stability of PGC-1α.

Clearly, we cannot ascribe the negative regulatory effects of MKP-1 on PGC-1α as the sole contributing mechanism for the resistance to diet-induced obesity in *mkp-1*$^{-/-}$ mice. However, based on the evidence provided in other studies — in which PGC-1α was overexpressed specifically in skeletal muscle (22), or deleted in skeletal muscle (23) — it is not unreasonable to propose that the increased levels of PGC-1α seen in *mkp-1*$^{-/-}$ mice are sufficient to account for the observed changes at the level of myofiber composition after HFD feeding. Interestingly, despite the improved oxidative myofiber capacity in the *mkp-1*$^{-/-}$ mice, these mice do not exhibit improved insulin sensitivity (14). It is likely that other contributing factors independent of PGC-1α supersede its anticipated protective effects on the actions of insulin and glucose homeostasis. Although there is consensus that PGC-1α is clearly responsible for promoting mitochondrial biogenesis and oxidative myofiber formation, a precise understanding of its role in glucose homeostasis is still evolving (52–54).

Collectively, the data presented herein suggest that MKP-1 participates in a negative feedback loop in skeletal muscle to limit p38 MAPK–mediated phosphorylation and regulation of PGC-1α activity (Figure 7D). Under basal conditions, MKP-1 is expressed at low levels that are permissive for p38 MAPK–mediated signaling to PGC-1α. In response to HFD feeding, MKP-1 becomes overexpressed and impairs p38 MAPK–mediated phosphorylation of PGC-1α, resulting in downregulation of PGC-1α and loss of skeletal muscle oxidative capacity. Obesity and insulin resistance have been proposed to be associated with a loss of oxidative myofiber composition as a result of downregulation of genes involved in mitochondrial oxidation (24–26). *Ppargc1a* is one of the target genes downregulated by FAs that is central to the loss of skeletal muscle oxidative capacity (26, 55). Therefore, our present findings implicate MKP-1 as a target that contributes to the loss of PGC-1α activity in response to HFD feeding. Finally, because PGC-1α dysfunction has been associated with other human diseases, such as neurological (56) and skeletal muscle diseases (57), the results presented here may have broader implications for the role played by MKP-1 in pathophysiological signaling and possibly pharmacological targeting for the treatment of obesity.

Methods

Maintenance of mice and metabolic calorimetry. The present studies in mice were reviewed and approved by the Institutional Animal Care and Use Committee of Yale University School of Medicine. Mice containing a disruption within exon 2 of MKP-1 (31) were backcrossed 8 times onto C57BL6/J mice obtained from Jackson Laboratories. All experiments were performed with age-matched males from heterozygous breeder pairs. Mice were maintained on chow feed 2018 (Harlan Teklad). For HFD studies, male mice were weaned onto TD 93075 diet (Harlan Teklad) for 16 weeks. Genotyping was performed as previously described (14) and additionally using the following primer sets: WT forward, 5′-CTGACAGTGCAGAATCCGGA-3′; WT reverse, 5′-CTATGAAGTCAATAGCCTCGTTGA-3′; KO forward, 5′-ACTGTGTCGGTGGTGCTAATGAGA-3′; KO reverse, 5′-TACCGGTGGATGTGGAATGTGT-3′. Metabolic calorimetry was performed as previously described (14). Whole body fat and lean mass and metabolic measurements for locomotor activity, food consumption, and energy expenditure were performed as previously described (14).

Skeletal muscle staining and quantitation of immunohistochemical analyses. TA muscle was dissected from mice fed chow or HFD for 16 weeks after weaning. Unperfused, unfixed muscle was frozen in OCT and sectioned into 10-μm sections. Positive staining myofibers were quantitated by manual counting in TA sections from 300–1,000 individual myofibers per animal; each group consisted of 3–8 mice. NADH dehydrogenase activity was determined by a 30-minute incubation at 37°C with 1.5 mM NADH and 1.5 mM Nitro blue tetrazolium in 0.2 M Tris (58). Succinate dehydrogenase activity was determined by a 1-hour incubation at 37°C with 45 mM succinate and 1 mg/ml Nitro blue tetrazolium in 100 mM phosphate buffer, pH 7.6, containing KCN, EDTA, and phenazine methosulfate. Cytochrome oxidase activity was determined by a 1-hour incubation at room temperature with 1 mg/ml cytochrome C and 0.5 mg/ml DAB in 50 mM phosphate buffer containing sucrose and catalase (all muscle staining reagents were from Sigma-Aldrich). MHC staining was performed with antibodies toward MHCI (Sigma-Aldrich), MHCIIA (clone SC-71), MHCIIX (clone 6H1, a gift from L. Leinwand, University of Colorado Health Sciences Center, Denver, Colorado, USA), or MHCIIB (clone BF-F3) using Vector labs ABC kit for mouse IgG or IgM and DAB reagent (Vector Labs) according to the manufacturer's instructions.

RNA isolation and analysis. RNA was isolated from C2C12 myoblasts, TA muscle, or quadriceps muscle using TRIzol reagent (Invitrogen) according to the manufacturer's instructions. RNA was reverse transcribed with Applied Biosystems Reverse Transcription Reagents, and RT-PCR was performed using SYBR green PCR master mix (Applied Biosystems) on ABI Prism 7500 with the following primer pairs: PGC-1α, 5′-CCCTGCCATTGTTAAGACC-3′ and 3′-CTGCTGCTGTTCCTGTTTTC-5′; MKP-1, 5′-ATTTGCTGAACTCGGCACATTCGG-3′ and 3′-GGCAAGCGAAGAAACTGCCTCAAA-5′; 18S, 5′-GACACGGACAGGATTGACAGATTG-3′ and 3′-AAATCGCTCCACCAACTAAGAACG-5′. Data were quantitated using the ΔCt method and expressed relative to 18S. For Northern blotting, RNA was electrophoresed on a 1% agarose formaldehyde gel and transferred to Zeta probe membrane (BioRad). MKP-1 cDNA or GAPDH (5′-GGGTGGAGCCAAACGGGTC-3′ and 3′-GGAGTTGCTGTTGAAGTCGCA-5′) was used as a probe and was labeled with random primer labeling (Stratagene).

Luciferase activity assays. C2C12 myoblasts were cultured in DMEM (Gibco; Invitrogen) supplemented with 10% FBS (Gemini), 1% penicillin and streptomycin (Sigma-Aldrich), and 1% sodium pyruvate (Gibco; Invitrogen) at 37°C. Luciferase assays were performed using the dual luciferase reporter assay system (Promega) in triplicate. Luciferase values were normalized to TK-Renilla values as a control for transfection efficiency. Plasmids (PGC-1α plasmids provided by B. Spiegelman, Dana Farber Cancer Institute, Boston, Massachusetts, USA) were transfected with Lipofectamine 2000 (Invitrogen) according to the manufacturer's instructions. PGC-1α–luciferase (plasmid no. 8887;

Addgene; ref. 59) was analyzed 48 hours after transfection and normalized to pGL3 alone. PGC-1α–GAL4 (plasmid no. 8892; Addgene; ref. 60) experiments were replated 16 hours after transfection, starved overnight in 0.5% FBS, and stimulated for 24 hours with 10 ng/ml TNF-α (Calbiochem). Cells transfected with a –1.4 kb fragment of the MKP-1 promoter fused to luciferase (61) were replated 16 hours after transfection, starved overnight in 0.5% FBS, and stimulated for 16 hours with vehicle, 500 μM palmitate (Sigma-Aldrich), 500 μM palmitoleic acid (Sigma-Aldrich), 500 μM eicosapentaenoic acid (EPA; Calbiochem), or 2.5 μg/ml anisomycin (Sigma-Aldrich). For siRNA experiments, C2C12 myoblasts were transfected either with 50 nM nontargeting siRNA or MKP-1 siRNA (Santa Cruz Biotechnology Inc.) with RNAiMax transfection reagent (Invitrogen) and replated 24 hours after transfection.

FA stimulation experiments. Palmitate (Sigma-Aldrich), palmitoleic acid (Sigma-Aldrich), stearic acid (Sigma-Aldrich), oleic acid (Cayman Chemical), and EPA (Calbiochem) were conjugated to 10% FA-free BSA (Sigma-Aldrich) in DMEM for 1–2 h at 55°C. Lipids were then diluted 10-fold into DMEM (in the absence of serum) prior to treatment to achieve a final lipid concentration of 100, 400, or 500 μM. Cells were starved for 2 hours or overnight prior to stimulation. For MAPK inhibitor experiments, cells were treated with 5 μM SB203580 (Calbiochem), 10 μM SP600125 (Calbiochem), or 20 μM U0126 (Sigma-Aldrich) for 1 hour prior to stimulation for 30 minutes with palmitate. Cell death was calculated after 30 minutes of FA treatment as the percentage of total cells positive for trypan blue (Gibco; Invitrogen). RNA and luciferase were assessed as described above.

Transient transfections and immunoblotting. C2C12 myoblasts were cultured as above and transfected with the following plasmids: Flag-tagged PGC-1α (plasmid no. 1026; Addgene; ref. 62), pcDNA3-MKP-1, MKK6EE, pcDNA3-MKK7DD, and pMCL1-Mek Δn3 ×7 with Lipofectamine 2000. For stimulation experiments, cells were replated 24 hours after transfection into 50 nM siRNA as described above. Cells were starved for 2 hours and stimulated with 10 ng/ml TNF-α. Cells and TA muscle were lysed in 20 mM HEPES, 150 mM NaCl, 2 mM EDTA, 1% triton, 0.1% SDS, 10% glycerol, 1 mM DTT, and 0.5% sodium deoxycholic acid. Lysis buffer was supplemented with protease and phosphatase inhibitors (5 μg/ml leupeptin, 5 μg/ml aprotinin, 1 μg/ml pepstatin A, 1 mM PMSF, 1 mM benzamidine, 1 mM Na_3VO_4, and 10 mM NaF). Lysates were clarified by centrifugation, and protein concentration was assessed by Bradford assay (Coomassie Protein Reagent; Pierce). Flag-tagged proteins were immunoprecipitated with monoclonal anti-Flag M2 antibodies (Sigma-Aldrich), and lysates were run on an SDS-PAGE gel, transferred to Immobilon-P membrane, and immunoblotted with PGC-1α (H300), MKP-1 (M18), p38 MAPK, Na/K ATPase (Santa Cruz Biotechnology Inc.), phospho–p38 MAPK, phospho-JNK, JNK (Cell Signaling Technology), or Lamin-β1 (Abcam). Phospho peptides representing phospho-Ser265 (LPLTPE-pS-PNDPKGSP) and phospho-Thr298 (AGLTPPT-pT-PPHKANQ) of PGC-1α were synthesized and used for antibody production (Proteintech Group Inc.).

Nuclear fractionation experiments. Skeletal muscle was enriched into cytoplasmic and nuclear fractions using the Nuclei Enrichment Kit for Tissue (Pierce) with a modified protocol. Muscle was cut into small pieces in cold PBS and subsequently homogenized on ice in a 1:1 mix of reagents A and B containing protease and phosphatase inhibitors (buffer 1) with a polytron homogenizer at low speed. The resulting homogenate was spun at 1,000 *g* for 10 minutes to obtain a crude nuclear pellet, and the supernatant was kept as the cytosolic fraction. The nuclear pellet was resuspended in 30% optiprep (reagent C) diluted in buffer 1 with additional protease and phosphatase inhibitors. The resulting suspension was spun at 10,000 *g* for 20 minutes to obtain a nuclear pellet. The supernatant was discarded, and the pellet was resuspended in T-PER tissue lysis buffer (Pierce) supplemented with protease and phosphatase inhibitors, 1 mM DTT, and 0.3% SDS. Cytoplasmic and nuclear fractions were clarified at 20,817 *g* for 15 minutes prior to protein determination with the reducing agent–compatible BCA assay (Pierce), SDS-PAGE electrophoresis, and immunoblotting.

Pulse-chase analysis. C2C12 myoblasts were transfected with Flag-tagged PGC-1α and with MKP-1 siRNA as above. Cells were starved in cysteine- and methione-free DMEM (Gibco; Invitrogen) supplemented with L-glutamine, 10% dialyzed calf serum, 1% penicillin/streptomycin, and 1% sodium pyruvate for 3 hours. Cells were pulsed with 200 μCi Express protein labeling mix (Perkin-Elmer) for 1 hour at 37°C and then chased with 2 ml complete DMEM supplemented with 2 mM methione and cysteine. Cells were lysed, and anti-Flag antibodies were used to immunoprecipitate PGC-1α.

Acyl-coA analysis. The extraction procedure for acyl-CoA species was adapted from methods described previously (63). Approximately 40 mg of plantaris muscle tissue isolated from *mkp-1*$^{+/+}$ mice fed chow or HFD for 16 weeks was homogenized with C17:0 acyl-CoA-ester internal standard. After purification using Oligonucleotide Purification Cartridges (Applied Biosystems), the medium, long-chain, and very-long-chain acyl-CoA fractions were eluted with 60% acetonitrile. Lipid metabolite extracts were subjected to liquid chromatography/mass spectrometry/mass spectrometry analysis. A turbo ionspray source was interfaced with an API 3000 tandem mass spectrometer (Applied Biosystems) in conjunction with a Shimadzu Prominence HPLC system (Shimadzu Scientific Instruments). Total acyl-CoA content was expressed as the sum of individual species.

Statistics. Statistical analysis of growth curves was performed with 1-way ANOVA with Bonferroni post-test using GraphPad Instat software (GraphPad Software). Statistical analyses between *mkp-1*$^{+/+}$ and *mkp-1*$^{-/-}$ mice were calculated by 2-tailed, unpaired Student's *t* test assuming equal variances using Microsoft Excel Analysis Tool (Microsoft Corp.). The relative expression of proteins and mRNAs was quantitated by densitometry using LabWorks 4.0 software (UVP Inc.). Analysis of PGC-1α $t_{1/2}$ was determined by linear regression analysis using GraphPad Prism (GraphPad Software). A *P* value of 0.05 or less was considered significant.

Acknowledgments

We thank Leslie Leinwand for MHCIIX monoclonal antibody and Bruce Spiegelman for PGC-1α plasmids. This work was supported by the PhRMA Foundation and NIH grant T32 DK07356 to R.J. Roth; by NIH grants AR46524 and DK75776 to A.M. Bennett; by NIH grants DK40936, P30 DK45735, and U24 DK-76169 to G.I. Shulman; and by a VA Merit Award to V.T. Samuel.

Received for publication February 26, 2009, and accepted in revised form September 23, 2009.

Address correspondence to: Anton M. Bennett, Yale University School of Medicine, Department of Pharmacology, SHM B226D, 333 Cedar Street, New Haven, Connecticut 06520, USA. Phone: (203) 737-2441; Fax: (203) 737-2738; E-mail: anton.bennett@yale.edu.

The authors deeply regret the tragic death of Annie M. Le, whose life was cut short in a homicide September 8, 2009.

1. Raman, M., Chen, W., and Cobb, M.H. 2007. Differential regulation and properties of MAPKs. *Oncogene.* **26**:3100–3112.
2. Weston, C.R., and Davis, R.J. 2007. The JNK signal transduction pathway. *Curr. Opin. Cell Biol.* **19**:142–149.
3. Cuenda, A., and Rousseau, S. 2007. p38 MAP-Kinases pathway regulation, function and role in human diseases. *Biochim. Biophys. Acta.* **1773**:1358–1375.
4. Murphy, L.O., and Blenis, J. 2006. MAPK signal specificity: the right place at the right time. *Trends Biochem. Sci.* **31**:268–275.
5. Weston, C.R., and Davis, R.J. 2007. The JNK signal transduction pathway. *Curr. Opin. Cell Biol.*

19:142–149.
6. Dickinson, R.J., and Keyse, S.M. 2006. Diverse physiological functions for dual-specificity MAP kinase phosphatases. *J. Cell Sci.* **119**:4607–4615.
7. Boutros, T., Chevet, E., and Metrakos, P. 2008. Mitogen-activated protein (MAP) kinase/MAP kinase phosphatase regulation: roles in cell growth, death, and cancer. *Pharmacol. Rev.* **60**:261–310.
8. Karlsson, M., Mandl, M., and Keyse, S.M. 2006. Spatio-temporal regulation of mitogen-activated protein kinase (MAPK) signalling by protein phosphatases. *Biochem. Soc. Trans.* **34**:842–845.
9. Cuevas, B.D., Abell, A.N., and Johnson, G.L. 2007. Role of mitogen-activated protein kinase kinase kinases in signal integration. *Oncogene.* **26**:3159–3171.
10. Keyse, S.M. 2008. Dual-specificity MAP kinase phosphatases (MKPs) and cancer. *Cancer Metastasis Rev.* **27**:253–261.
11. Jeffrey, K.L., Camps, M., Rommel, C., and Mackay, C.R. 2007. Targeting dual-specificity phosphatases: manipulating MAP kinase signalling and immune responses. *Nat. Rev. Drug Discov.* **6**:391–403.
12. Liu, Y., Shepherd, E.G., and Nelin, L.D. 2007. MAPK phosphatases [mdash] regulating the immune response. *Nat. Rev. Immunol.* **7**:202–212.
13. Owens, D.M., and Keyse, S.M. 2007. Differential regulation of MAP kinase signalling by dual-specificity protein phosphatases. *Oncogene.* **26**:3203–3213.
14. Wu, J.J., et al. 2006. Mice lacking MAP kinase phosphatase-1 have enhanced MAP kinase activity and resistance to diet-induced obesity. *Cell Metab.* **4**:61–73.
15. Bassel-Duby, R., and Olson, E.N. 2006. Signaling pathways in skeletal muscle remodeling. *Annu. Rev. Biochem.* **75**:19–37.
16. Zierath, J.R., and Hawley, J.A. 2004. Skeletal muscle fiber type: influence on contractile and metabolic properties. *PLoS Biol.* **2**:e348.
17. Zurlo, F., Larson, K., Bogardus, C., and Ravussin, E. 1990. Skeletal muscle metabolism is a major determinant of resting energy expenditure. *J. Clin. Invest.* **86**:1423–1427.
18. He, J., Watkins, S., and Kelley, D.E. 2001. Skeletal muscle lipid content and oxidative enzyme activity in relation to muscle fiber type in type 2 diabetes and obesity. *Diabetes.* **50**:817–823.
19. Simoneau, J.A., Veerkamp, J.H., Turcotte, L.P., and Kelley, D.E. 1999. Markers of capacity to utilize fatty acids in human skeletal muscle: relation to insulin resistance and obesity and effects of weight loss. *FASEB J.* **13**:2051–2060.
20. Handschin, C., and Spiegelman, B.M. 2006. Peroxisome proliferator-activated receptor {gamma} coactivator 1 coactivators, energy homeostasis, and metabolism. *Endocr. Rev.* **27**:728–735.
21. Handschin, C., and Spiegelman, B.M. 2008. The role of exercise and PGC1alpha in inflammation and chronic disease. *Nature.* **454**:463–469.
22. Lin, J., et al. 2002. Transcriptional co-activator PGC-1 alpha drives the formation of slow-twitch muscle fibres. *Nature.* **418**:797–801.
23. Handschin, C., et al. 2007. Skeletal muscle fiber-type switching, exercise intolerance, and myopathy in PGC-1alpha muscle-specific knock-out animals. *J. Biol. Chem.* **282**:30014–30021.
24. Mootha, V.K., et al. 2003. PGC-1[alpha]-responsive genes involved in oxidative phosphorylation are coordinately downregulated in human diabetes. *Nat. Genet.* **34**:267–273.
25. Patti, M.E., et al. 2003. Coordinated reduction of genes of oxidative metabolism in humans with insulin resistance and diabetes: Potential role of PGC1 and NRF1. *Proc. Natl. Acad. Sci. U. S. A.* **100**:8466–8471.
26. Sparks, L.M., et al. 2005. A high-fat diet coordinately downregulates genes required for mitochondrial oxidative phosphorylation in skeletal muscle. *Diabetes.* **54**:1926–1933.
27. Crunkhorn, S., et al. 2007. Peroxisome proliferator activator receptor {gamma}çesity: potential pathogenic role of saturated fatty acids and p38 mitogen-activated protein kinase activation. *J. Biol. Chem.* **282**:15439–15450.
28. Coll, T., et al. 2006. Palmitate-mediated downregulation of peroxisome proliferator-activated receptor-gamma coactivator 1alpha in skeletal muscle cells involves MEK1/2 and nuclear factor-kappaB activation. *Diabetes.* **55**:2779–2787.
29. Puigserver, P., et al. 2001. Cytokine stimulation of energy expenditure through p38 MAP kinase activation of PPARgamma coactivator-1. *Mol. Cell.* **8**:971–982.
30. Akimoto, T., et al. 2005. Exercise stimulates Pgc-1{alpha} transcription in skeletal muscle through activation of the p38 MAPK pathway. *J. Biol. Chem.* **280**:19587–19593.
31. Dorfman, K., et al. 1996. Disruption of the *erp/mkp-1* gene does not affect mouse development: normal MAP kinase activity in ERP/MKP-1-deficient fibroblasts. *Oncogene.* **13**:925–931.
32. Kwak, S.P., and Dixon, J.E. 1995. Multiple dual specificity protein tyrosine phosphatases are expressed and regulated differentially in liver cell lines. *J. Biol. Chem.* **270**:1156–1160.
33. Cao, H., et al. 2008. Identification of a lipokine, a lipid hormone linking adipose tissue to systemic metabolism. *Cell.* **134**:933–944.
34. Shi, H., et al. 2006. TLR4 links innate immunity and fatty acid-induced insulin resistance. *J. Clin. Invest.* **116**:3015–3025.
35. Fan, M., et al. 2004. Suppression of mitochondrial respiration through recruitment of p160 myb binding protein to PGC-1alpha: modulation by p38 MAPK. *Genes Dev.* **18**:278–289.
36. Knutti, D., Kressler, D., and Kralli, A. 2001. Regulation of the transcriptional coactivator PGC-1 via MAPK-sensitive interaction with a repressor. *Proc. Natl. Acad. Sci. U. S. A.* **98**:9713–9718.
37. Wells, G.D., Noseworthy, M.D., Hamilton, J., Tarnopolski, M., and Tein, I. 2008. Skeletal muscle metabolic dysfunction in obesity and metabolic syndrome. *Can. J. Neurol. Sci.* **35**:31–40.
38. Kelley, D.E., Goodpaster, B., Wing, R.R., and Simoneau, J.A. 1999. Skeletal muscle fatty acid metabolism in association with insulin resistance, obesity, and weight loss. *Am. J. Physiol.* **277**:E1130–E1141.
39. Kim, J.Y., Hickner, R.C., Cortright, R.L., Dohm, G.L., and Houmard, J.A. 2000. Lipid oxidation is reduced in obese human skeletal muscle. *Am. J. Physiol. Endocrinol. Metab.* **279**:E1039–E1044.
40. Chi, H., et al. 2006. Dynamic regulation of pro- and anti-inflammatory cytokines by MAPK phosphatase 1 (MKP-1) in innate immune responses. *Proc. Natl. Acad. Sci. U. S. A.* **103**:2274–2279.
41. Garcia-Roves, P., et al. 2007. Raising plasma fatty acid concentration induces increased biogenesis of mitochondria in skeletal muscle. *Proc. Natl. Acad. Sci. U. S. A.* **104**:10709–10713.
42. Turner, N., et al. 2007. Excess lipid availability increases mitochondrial fatty acid oxidative capacity in muscle: evidence against a role for reduced fatty acid oxidation in lipid-induced insulin resistance in rodents. *Diabetes.* **56**:2085–2092.
43. Hancock, C.R., et al. 2008. High-fat diets cause insulin resistance despite an increase in muscle mitochondria. *Proc. Natl. Acad. Sci. U. S. A.* **105**:7815–7820.
44. Bonnard, C., et al. 2008. Mitochondrial dysfunction results from oxidative stress in the skeletal muscle of diet-induced insulin-resistant mice. *J. Clin. Invest.* **118**:789–800.
45. Choi, C.S., et al. 2007. Overexpression of uncoupling protein 3 in skeletal muscle protects against fat-induced insulin resistance. *J. Clin. Invest.* **117**:1995–2003.
46. Cha, S.H., Rodgers, J.T., Puigserver, P., Chohnan, S., and Lane, M.D. 2006. Hypothalamic malonyl-CoA triggers mitochondrial biogenesis and oxidative gene expression in skeletal muscle: Role of PGC-1alpha. *Proc. Natl. Acad. Sci. U. S. A.* **103**:15410–15415.
47. Jager, S., Handschin, C., St-Pierre, J., and Spiegelman, B.M. 2007. AMP-activated protein kinase (AMPK) action in skeletal muscle via direct phosphorylation of PGC-1alpha. *Proc. Natl. Acad. Sci. U. S. A.* **104**:12017–12022.
48. Li, X., Monks, B., Ge, Q., and Birnbaum, M.J. 2007. Akt/PKB regulates hepatic metabolism by directly inhibiting PGC-1alpha transcription coactivator. *Nature.* **447**:1012–1016.
49. Gerhart-Hines, Z., et al. 2007. Metabolic control of muscle mitochondrial function and fatty acid oxidation through SIRT1/PGC-1alpha. *EMBO J.* **26**:1913–1923.
50. Teyssier, C., Ma, H., Emter, R., Kralli, A., and Stallcup, M.R. 2005. Activation of nuclear receptor coactivator PGC-1alpha by arginine methylation. *Genes Dev.* **19**:1466–1473.
51. Sano, M., et al. 2007. Intramolecular control of protein stability, subnuclear compartmentalization, and coactivator function of peroxisome proliferator-activated receptor {gamma} coactivator 1{alpha}. *J. Biol. Chem.* **282**:25970–25980.
52. Choi, C.S., et al. 2008. Paradoxical effects of increased expression of PGC-1alpha on muscle mitochondrial function and insulin-stimulated muscle glucose metabolism. *Proc. Natl. Acad. Sci. U. S. A.* **105**:19926–19931.
53. Leone, T.C., et al. 2005. PGC-1alpha deficiency causes multi-system energy metabolic derangements: muscle dysfunction, abnormal weight control and hepatic steatosis. *PLoS Biol* **3**:e101.
54. Benton, C.R., et al. 2008. Modest PGC-1alpha overexpression in muscle in vivo is sufficient to increase insulin sensitivity and palmitate oxidation in subsarcolemmal, not intermyofibrillar, mitochondria. *J. Biol. Chem.* **283**:4228–4240.
55. Richardson, D.K., et al. 2005. Lipid infusion decreases the expression of nuclear encoded mitochondrial genes and increases the expression of extracellular matrix genes in human skeletal muscle. *J. Biol. Chem.* **280**:10290–10297.
56. Lin, J., et al. 2004. Defects in adaptive energy metabolism with CNS-linked hyperactivity in PGC-1alpha null mice. *Cell.* **119**:121–135.
57. Handschin, C., et al. 2007. PGC-1{alpha} regulates the neuromuscular junction program and ameliorates Duchenne muscular dystrophy. *Genes Dev.* **21**:770–783.
58. Jackson, K.A., Snyder, D.S., and Goodell, M.A. 2004. Skeletal muscle fiber-specific green autofluorescence: potential for stem cell engraftment artifacts. *Stem Cells.* **22**:180–187.
59. Handschin, C., Rhee, J., Lin, J., Tarr, P.T., and Spiegelman, B.M. 2003. An autoregulatory loop controls peroxisome proliferator-activated receptor gamma coactivator 1alpha expression in muscle. *Proc. Natl. Acad. Sci. U. S. A.* **100**:7111–7116.
60. Puigserver, P., et al. 1998. A cold-inducible coactivator of nuclear receptors linked to adaptive thermogenesis. *Cell.* **92**:829–839.
61. Kwak, S.P., Hakes, D.J., Martell, K.J., and Dixon, J.E. 1994. Isolation and characterization of a human dual specificity protein-tyrosine phosphatase gene. *J. Biol. Chem.* **269**:3596–3604.
62. Monsalve, M., et al. 2000. Direct coupling of transcription and mRNA processing through the thermogenic coactivator PGC-1. *Mol. Cell.* **6**:307–316.
63. Neschen, S., et al. 2002. Contrasting effects of fish oil and safflower oil on hepatic peroxisomal and tissue lipid content. *Am. J. Physiol. Endocrinol. Metab.* **282**:E395–E401.